JPE 17-5-13

https://doi.org/10.6113/JPE.2017.17.5.1256
ISSN(Print): 1598-2092 / ISSN(Online): 2093-4718

A Fault Tolerant Structure and Control Strategy for Electromagnetic Stirring Supplies

Yan Li[*,**], An Luo[*], Xinxing Xiang[†], Yandong Chen[*], Zhixing He[*], Fayun Zhou[*], and Zhiyong Chen[*]

[*,†]College of Electrical and Information Engineering, Hunan University, Changsha, China
[**]School of Information Science and Engineering, Central South University, Changsha, China

Abstract

A fault tolerant structure and its corresponding control strategy for electromagnetic stirring power supplies are proposed in this paper. The topology structure of the electromagnetic stirring power supply contains two-stages. The fore-stage is the PWM rectifier. The back-stage is the fault tolerant inverter, which is a two-phase three-bridge orthogonal inverter circuit while operating normally. When the power switch devices in the inverter are faulty, the structure of the inverter is reconfigured. The two-phase half bridge inverter circuit is constructed with the remaining power switch devices and DC-link capacitors to keep the system operating after cutting the faulty power switch devices from the system. The corresponding control strategy is proposed to let the system work under both normal and fault conditions. The reliability of the system is improved and the requirement of the electromagnetic stirring process is met. Finally, simulation and experimental results verify the feasibility of the proposed fault tolerant structure and corresponding control strategy.

Key words: Electromagnetic stirring, Fault tolerant structure, Two-phase half bridge, Two-phase orthogonal inverter

I. INTRODUCTION

In the high quality special steel process and smelting industry, continuous casting electromagnetic stirring technology has become the most effective way to improve the quality and yield of continuous casting steel [1]. As the key equipment of continuous casting electromagnetic stirring, the current quality and response rate of the electromagnetic stirring power supply directly influence the quality of the cast steel, which is of great significant to enhance military ships, bridges, buildings, luxury cars and other manufacturing processes [2], [3].

At present, the two-phase orthogonal inverter is generally used in the electromagnetic stirring power supplies of iron and steel continuous casting. Two-phase orthogonal currents are supplied to the induction coil and electromagnetic force is excited. Therefore, the steel liquid rotation movement forms. The stirring method has the advantages of magnetic field energy concentration, low stirring power and high winding energy efficiency [4]. In terms of the topological structure of electromagnetic stirring power supplies, the two-stage structure is generally adopted. In the fore-stage, three-phase alternating current is converted into a stable DC by an uncontrollable rectifier [5], [6]. Due to the inductive load of the electromagnetic stirring power supply, less active power is consumed and the load power is mainly reactive power. As a result, the power factor is low and the harmonic content is high in the fore-stage. Two single-phase inverters are used in the back-stage, which can be separately controlled to convert DC into two-phase orthogonal AC power [7]. This structure has the advantages of a simple control and a high utilization rate of the DC voltage. However, a large number of devices are need and its cost is high. Thus, the authors of [8] proposed a two-phase orthogonal inverter with two-bridges. Each bridge and the DC side capacitors constitute a half bridge inverter to realize the two orthogonal output voltages. Although the number of devices is reduced, the DC voltage utilization rate is low and the two capacitors in the DC side needs to be balanced. Therefore, the authors of [4], [9] proposed a two-phase orthogonal inverter structure with three-bridges. Two of the bridges are for independent switching, and the third bridge is a public bridge. The

Manuscript received Sep.19, 2016; accepted May 22, 2017
Recommended for publication by Associate Editor Bon-Gwan Gu.
[†]Corresponding Author: zkdqxxx@163.com
Tel: +86-731-8882-3964, Hunan University
[*]College of Electrical and Information Eng., Hunan Univ., China
[**]School of Information Science and Eng., Central South Univ., China

two-phase orthogonal output can be realized by an appropriate control method.

In [10], the current closed loop proportional control was used to generate a modulation wave. Then the pulse width modulation method was used to generate a driving signal to drive the output of the switch. In order to improve the utilization ratio of the DC voltage, a space vector modulation method for four leg two-phase quadrature inverters was proposed in [11]. The SVM for a two-phase orthogonal inverter was proposed in [12]. However, the two-phase orthogonal current of the electromagnetic stirring power supply varies frequently in positive and negative alternations. The dynamic tracking performance of the output current is high. The closed loop control of the output current is controlled by the conventional method, which has a slow dynamic response. Therefore, the performance needs to be improved.

The most important part of an electromagnetic stirring power supply is the inverter. The most common faults in the inverter are the power switch devices and its control circuit, which is not able to effectively deal with the reliability of the inverter. When the inverter is faulty, the whole system cannot work properly, which leads to unimaginable consequences. Therefore, the inverter needs to achieve fault tolerance.

A fault tolerant structure and its corresponding control method for electromagnetic stirring power supplies are proposed in this paper. The inverter topology in fault status is configured to keep the system running.

This paper is organized as follows. Section II is the proposed fault tolerant topology structure of an electromagnetic stirring power supply. Section III is the proposed system control strategy, which contains control methods for the fore-stage and the back-stage. Simulation and experimental results are shown in Section IV to evaluate the feasibility of the proposed topology structure, and the performance of the proposed control strategy. Section V concludes the paper.

II. Topology Structure of an Electromagnetic Stirring Supply

A. The Traditional Topology Structure of an Electromagnetic Stirring Supply

The traditional topology structure of an electromagnetic stirring power supply is shown in Fig.1. The structure is composed of two parts. The first part is the fore-stage, which is made up of a three-phase voltage type PWM rectifier circuit. The second part is the back stage, which is made up of a two-phase orthogonal inverter circuit. The electromagnetic stirrer is the load. Three-phase AC voltages are converted into a stable DC voltage by the three-phase PWM rectifier, which is the power supply of the back-stage inverter circuit. The DC voltage is converted into an AC voltage by the back-stage inverter to obtain the desired two-phase low frequency orthogonal current for the electromagnetic stirrer.

During the operating process, an electromagnetic stirrer

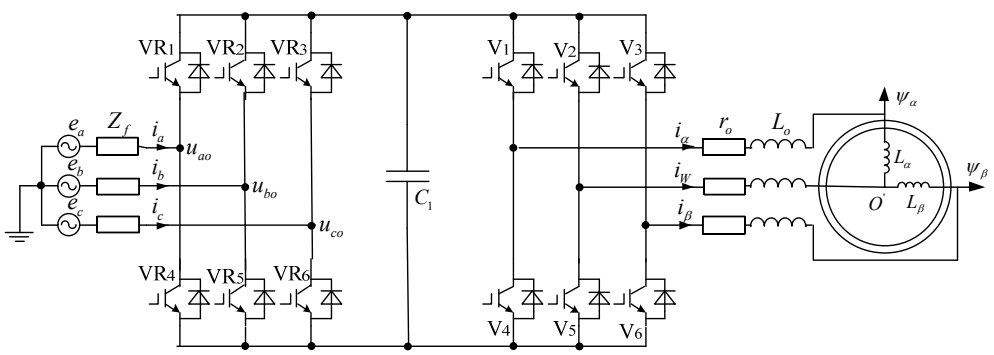

Fig. 1. Traditional topology of an electromagnetic stirring supply.

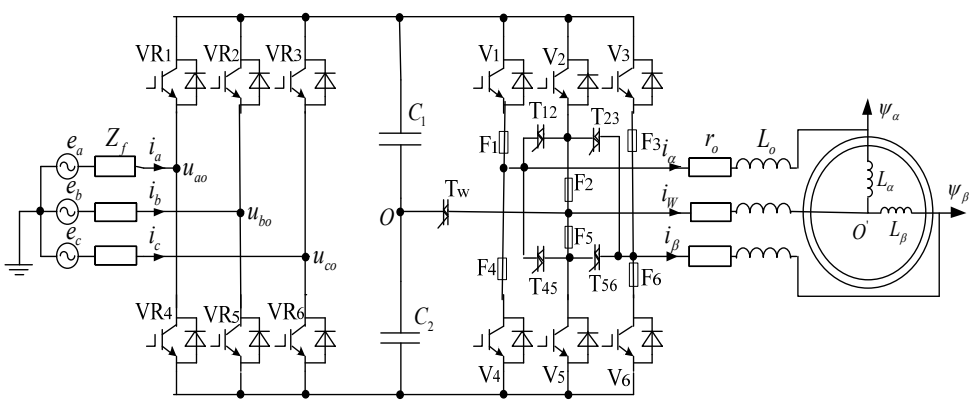

Fig. 2. Fault tolerance topology of an electromagnetic stirring power supply.

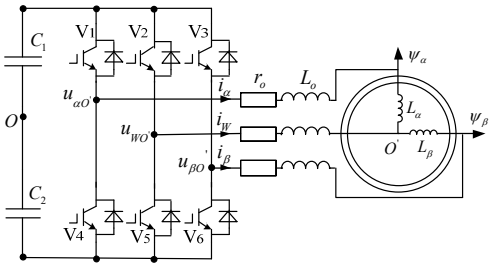

Fig. 3. Back-stage inverter circuit in the normal condition.

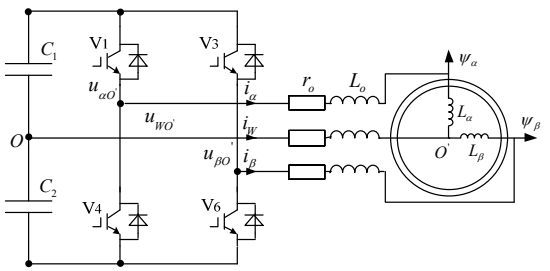

Fig. 4. Two-phase half bridge inverter circuit.

operates in three states: positive rotation, stop and reverse rotation. From Fig. 1 it can be seen that the back-stage inverter connects the load directly. Therefore, the power switch devices in the inverter are easy to be fault. If one or more of the power switch devices in the back-stage inverter is faulty, the whole system cannot work properly, which has catastrophic consequences. The fault tolerant topology structure of an electromagnetic stirring power supply is proposed in the paper.

B. The Fault Tolerant Topology Structure of an Electromagnetic Stirring Supply

The fault tolerant topology structure of an electromagnetic stirring power supply is shown in Fig. 2. The second part is a fault tolerant two-phase orthogonal inverter circuit as the back-stage. e_a, e_b and e_c are the grid voltages. VR_1-VR_6 constructs the three-phase rectifier circuit. C_1 and C_2 are the DC side capacitors. T_{12}, T_{23}, T_{45}, T_{56} and T_W are triacs. F_1-F_6 are fuses. C_1, C_2, T_{12}, T_{23}, T_{45}, T_{56}, T_W, F_1-F_6 and V_1-V_6 make up the fault tolerant circuit of the electromagnetic stirring power supply.

When the system works normally, the back-stage inverter circuit is shown in Fig. 3.

When the power switch devices in the back-stage circuit are faulty, the system can continue to operate normally by reconstructing the topology structure. For example, if the power switch device V_2 or V_5 or both are faulty, the reconstructed two-phase half bridge inverter circuit is shown in Fig. 4. A similar two-phase half bridge inverter circuit can be obtained if the other power switch devices are faulty.

The corresponding state table of triacs and fuses is shown in Table I.

In Table I, for example, if the power switch devices V_2 and V_5 are faulty, the fuses F_2 and F_4 are off (0). The triacs of T_{12}, T_{23}, T_{45} and T_{56} and the fuses F_1, F_3, F_5 and F_6 are on (1). Then the back-stage inverter is reconstructed as the two-phase half bridge inverter circuit.

TABLE I
STATE TABLE OF TRIACS AND FUSES

	V_1	V_2	V_3	V_4	V_5	V_6
F_1	0	1	1	1	1	1
F_2	0	0	0	0	0	0
F_3	1	1	0	1	1	1
F_4	1	1	1	0	1	1
F_5	0	0	0	0	0	0
F_6	1	1	1	1	1	0
T_{12}	1	0	0	0	0	0
T_{23}	0	0	1	0	0	0
T_{45}	0	0	0	1	0	0
T_{56}	0	0	0	0	0	1

The reconstructed two-phase half bridge inverter circuit has the advantages of a simple structure, high stability, reduced number of power switching devices and low cost. The series capacitors C_1 and C_2 have the same capacitance value, which provides the neutral point for the DC side voltage. Thus, the two coils have the same electrical potential.

III. THE CORRESPONDING CONTROL STRATEGY

The control aim of the fore-stage rectifier is to keep the total DC side voltage stable and to keep the input current waves as sinusoidal waves. The control aim of the back-stage inverter is to keep the two capacitors voltage equal and to let the output currents track the given reference currents. Therefore, there is no control coupling between the fore-stage and the back-stage. The two stages can be regarded as two relatively independent control objects.

The change of the DC side energy cannot be simply viewed as a whole. The control of the DC side voltage needs to control the balance of the two capacitor voltages and the total voltage.

A. The Control Method for the Fore-stage Rectifier

Although the fore-stage and back-stage can be regarded as two relatively independent control objects, there is asymmetry between one bridge and the other two bridges in the back-stage two-phase inverter. This leads to a second-order ripple voltage in the DC side capacitor. The harmonic current is contained in the output current of the fore-stage rectifier. A reduction of the second-order ripple voltage in the DC side can be presented by a power balance between the two stages.

The fluctuating power in the output power of the back-stage inverter is P_Z.

$$P_Z = \omega L_0 I_m^2 \cos(2\omega t) + r_0 I_m^2 \sin(2\omega t) \quad (1)$$

Where I_m and ω are the amplitude and angle frequency of the inverter output currents, respectively. In addition, the DC side voltage is:

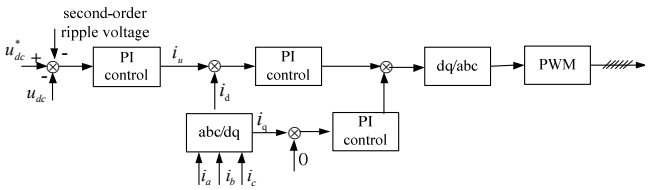

Fig. 5. Fore-stage rectifier control diagram.

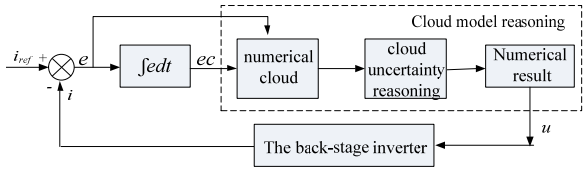

Fig. 6. Control process of the back-stage inverter based on the membership cloud model.

$$u_{dc} = U_d + \delta\sin(2\omega t + \varphi) \tag{2}$$

Where U_d is the DC component. The second-order ripple component is $\delta\sin(2\omega t + \varphi)$. The instantaneous power of the DC side capacitor is:

$$\begin{aligned} P_d &= u_{dc} C \frac{\mathrm{d}u_{dc}}{\mathrm{d}t} \\ &= C[U_d + \delta\sin(2\omega t + \varphi)]2\omega\delta\cos(2\omega t + \varphi) \\ &= 2\omega\delta C U_d \cos(2\omega t + \varphi) + \omega\delta^2 C \sin(4\omega t + 2\varphi) \end{aligned} \tag{3}$$

The total capacitance value of the DC side capacitor is *C*. Ignoring the fourth ripple component, according to the principle of the AC and DC power balance, there are:

$$2\omega\delta C U_d \cos(2\omega t + \varphi) = P_Z \tag{4}$$

The second-order ripple component of the DC side voltage is:

$$\delta\sin(2\omega t + \varphi) = \frac{\omega L I_m^2 \sin(2\omega t) - r I_m^2 \cos(2\omega t)}{2\omega C U_d} \tag{5}$$

It can be seen that the ripple voltage frequency is 2 times that of the output frequency. The ripple voltage is proportional to the square of the output current and is inversely proportional to the DC side capacitance voltage.

A control method with the DC side voltage control and the current control in the dq coordinate is proposed for the fore-stage rectifier, which eliminates ripple interference. The stability of the DC side voltage can be realized. The control diagram is shown in Fig. 5.

The change of the DC side voltage can be obtained as $\Delta u_{dc} = u_{dc}^* - u_{dc}$, where u_{dc}^* is the given DC side reference voltage. Then the DC side voltage tracking error Δu_d can be calculated as $\Delta u_d = \Delta u_{dc}$ $\delta\sin(2\omega t + \varphi)$. After regulation by the PI controller, the regulating signal i_u is:

$$i_u = k_P \Delta u_d + k_I \int \Delta u_d dt \tag{6}$$

Where k_P and k_I are the proportional coefficient and integral coefficient of the PI, respectively. Here k_P=0.8 and k_I=16 for the three PIs in Fig. 5.

The three-phase AC side currents are transformed into i_d and i_q in the dq coordinates. When the system works at a unity power factor, the reference currents i_{refd}=0 and i_{refd}=i_u are given in the dq coordinates.

In the proposed control method, DC-side voltage control is to maintain the stability of the DC side voltage. The function of the current control is to make the actual input current of the fore-stage rectifier capable of achieving unity power factor control.

B. The Control Method for the Back Stage Inverter

The output currents of the back-stage inverter directly drive the electromagnetic stirrer. In order to meet the positive and reverse driving requirements of the two-phase electromagnetic stirrer, the back-stage inverter should achieve fast and accurate tracking of the given reference currents. A current tracking control method based on the membership cloud model is proposed in the paper.

The membership cloud model is an effective method to represent and reason the knowledge for combining randomness with fuzziness, which can realize the natural transformation between a qualitative linguistic value and a quantitative value [13]-[17].

The control process of the back-stage inverter, based on the membership cloud model, is shown in Fig. 6.

It can be seen from Fig. 6 that the control idea of the control method based on the membership cloud model looks like the idea of a PI controller. However, they are different in nature. The membership cloud model reasoning includes three steps: numerical cloud, cloud uncertainty reasoning and numerical results.

The input signals of the membership cloud model reasoning are the error e and the error integral *ec* of the output current in the back-stage inverter. The output is *u*. The domain of each variable can be expressed as [X_{min}, X_{max}]. In this paper, the domains of *e* and *ec* are both [-10,10] and the domain of *u* is [-5,5]. The golden section method [18] is used to generate 7 clouds for each domain, which represent linguistic values. Take the error *e* as an example. The digital features of the cloud contain the expected value E_x, the entropy E_n and the super entropy H_e. The expected value E_x is the central value reflecting the information center value of the corresponding qualitative knowledge. The entropy E_n is a measure of the fuzzy degree of the qualitative concept reflecting the numerical range that can be accepted by this concept in the field of theory. *He* is the super entropy reflecting the degree of the discrete droplets.

The cloud model of the error *e* can be expressed as Ge (E_x, E_n, H_e). The 7-flower-cloud of *e* is obtained by Golden Segmentation as:

E-3="big negative error"

=Ge1(-10 3.34 0.42) ;
E-2="middle negative error"
= Ge2(-3.82 2.06 0.26) ;
E-1="small negative error"
= Ge3(-1.90 1.26 0.16) ;
E0="zero error"= Ge4(0 0.39 0.1) ;
E+1="small positive error"
= Ge5(1.9 1.26 0.16) ;
E+2="middle positive error"
= Ge6(3.82 2.06 0.26) ;
E+3="big positive error"
= Ge7(10 3.34 0.42)。

A positive cloud generator is constructed by these three numerical features. Assuming that the random function $R(Ex,\sigma)$ obeys a normal distribution, with a standard deviation of σ, a normal random entropy with E_n and H_e is generated.

$$E_n^{'} = R(En, He) \tag{7}$$

Then a normal random number x_i with the expected value of E_x and a standard deviation of $E_n^{'}$ is generated as:

$$x_i = R(Ex, E_n^{'}) \tag{8}$$

The membership equation with a normal distribution is finally obtained:

$$\mu_i = \exp\{\frac{-(x_i - Ex)^2}{2E_n^{'2}}\} \tag{9}$$

x_i with the degree of membership μ_i is a cloud droplet. A large number of x_i construct a cloud. A 7-flower-cloud of e is shown in Fig. 7. The number of droplets in every cloud is 1000. ec and u cloud model curves can be obtained in the same way.

GA((E_{xx} E_{xy}),(E_{nx} E_{ny}),(H_{ex}, H_{ey})) is a two-dimensional membership cloud model, if it meets:

$$E_{nx}^{'} = R(E_{nx}, H_{ex}) \tag{10}$$

$$E_{ny}^{'} = R(E_{ny}, H_{ey}) \tag{11}$$

$$\mu(x,y) = \exp\{\frac{-(x - E_{xx})^2}{2E_{nx}^{'2}} + \frac{-(y - E_{xy})^2}{2E_{ny}^{'2}}\} \tag{12}$$

Then the two-dimension cloud generator with an X-term is made as CG_A, if the given signals are put into Equ. (12). In other words:

$$\mu(e,ec) = \exp\{\frac{-(e - E_{xe})^2}{2E_{ne}^{'2}} + \frac{-(e_c - E_{xec})^2}{2E_{nec}^{'2}}\} \tag{13}$$

A two-dimension membership cloud model is shown in Fig. 8 at "if E_{+3} and EC_0". The cloud drop number is 1000. The number of droplets in every cloud is 1000.

Set μ be a given value. Then CG_B is a one-dimension cloud generator with Y-term, if it meets:

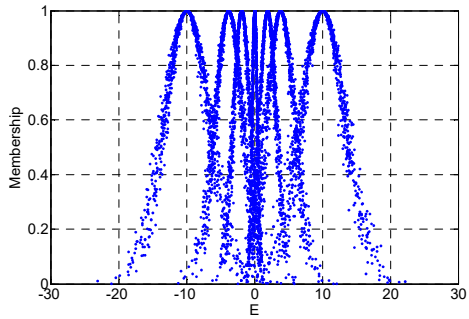

Fig. 7. Membership cloud of the error.

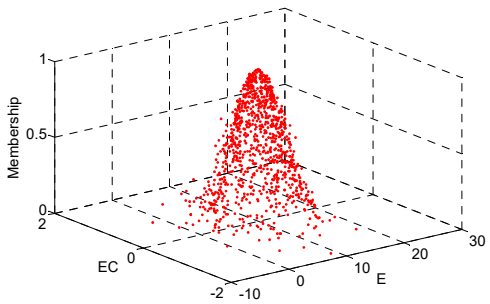

Fig. 8. Two-dimension membership cloud model.

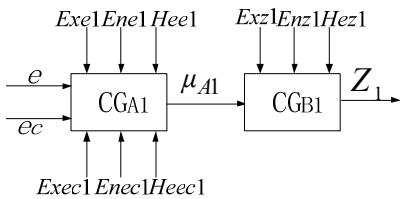

Fig. 9. Single rule generator.

$$E_n^{'} = R(E_n, H_e) \tag{14}$$

$$z_i = E_x \pm \sqrt{-2\ln(\mu)}E_n^{'} \tag{15}$$

Considering the two-condition and single output rule: "if A and B then Z", the single qualitative rule is constructed by the X-term two-dimensional cloud generator and the Y-term one-dimensional cloud generator, which is shown in Fig. 9.

The 3E rule is a rule that cloud drops at the universe of discourse U mainly contributing to the qualitative conception D are in the range of [E_x-$3E_n$, E_x+$3E_n$]. The 3E rule is given as follows. At the universe of discourse U, any value of Δx at X contributes to the qualitative conception D:

$$\Delta D \approx \frac{e^{-(x-E_x)^2/2E_n^2} \times \Delta x}{\sqrt{2\pi}E_n} \tag{16}$$

Obviously, there is:

$$\frac{\int_{E_x+3E_n}^{E_x-3E_n} e^{-(x-E_x)^2/2E_n^2} \times dx}{\sqrt{2\pi}E_n} = 99.74\% \tag{17}$$

Therefore, quantified data contributing to the qualitative conception D is mainly in the range of [E_x-$3E_n$, E_x+$3E_n$]. The other quantified data out of this region can be neglected. Thus,

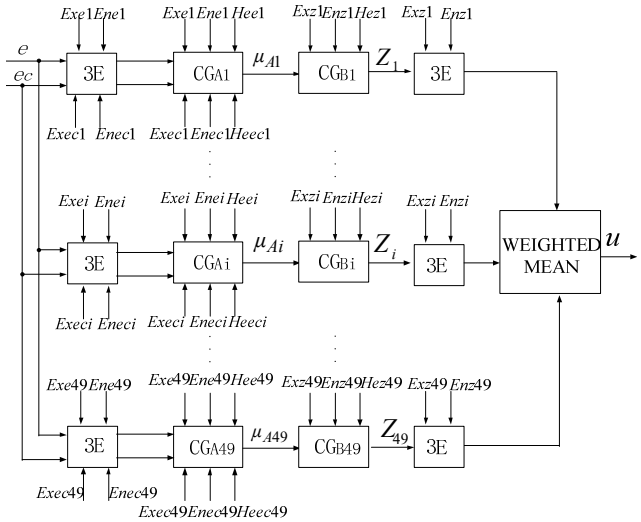

Fig. 10. Rule generator.

x should satisfy:

(1) $x \in [E_x - 3E_n, E_x + 3E_n]$

(2) $if\ x < E_x - 3E_n,\ x = E_x - 3E_n$

(3) $if\ x > E_x + 3E_n,\ x = E_x + 3E_n$

Multiple qualitative rules are constructed as shown in Fig. 10. CG_{Ai}, and CG_{Bi} are the two-dimension cloud generator with the X-term and the one-dimension cloud generator with the Y-term, respectively. The input and output signals should meet the requirements of the 3E rule in the rule generator.

In Fig. 10, after the input signals, which meet the requirements of the 3E rule for obtaining the corresponding linguistic value, the input signals stimulate the cloud generator of CG_{Ai} (i = 1, 2,..., n), where n=49. Each CG_{Ai} randomly produces a group of $\mu_{Ai} = \mu_{ij}$ (j = 1, 2,..., m) values, where m=1000. These values indicate that the qualitative rules are selected. z_i can be obtained by the corresponding CG_{Bi} to produce m drop(z_i , μ_{ij}) cloud drops. The k weighted mean of z_i meeting the requirements of the 3E rule is the output, that is:

$$u = \frac{\sum_{i=1}^{k} z_i \mu_{ij}}{\sum_{i=1}^{k} \mu_{ij}} \tag{18}$$

According to the working principle of the electromagnetic stirring, the phase α and phase β currents flowing through the electromagnetic stirrer are low frequency sine wave currents with equal amplitudes and a phase difference of 90 degrees. The given reference output currents of the back-stage inverter can be expressed as:

$$\begin{cases} i_\alpha^* = I^* \sin(\omega^* t) \\ i_\beta^* = I^* \cos(\omega * t) \\ i_w^* = -(i_\alpha^* + i_\beta^*) \end{cases} \tag{19}$$

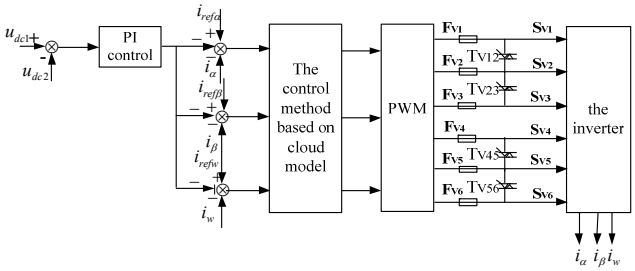

Fig. 11. Control diagram of the back-stage inverter.

TABLE II
ON-OFF RELATIONSHIP BETWEEN T_{V12}, T_{V23}, T_{V45}, T_{V56} AND THE POWER SWITCH DEVICES

	V_1	V_2	V_3	V_4	V_5	V_6
F_{V1}	1	1	1	1	1	1
F_{V2}	0	0	0	0	0	0
F_{V3}	1	1	1	1	1	1
F_{V4}	1	1	1	1	1	1
F_{V5}	0	0	0	0	0	0
F_{V6}	1	1	1	1	1	1
T_{v12}	1	0	0	0	0	0
T_{v23}	0	0	1	0	0	0
T_{v45}	0	0	0	1	0	0
T_{v56}	0	0	0	0	0	1

In Equ. (19), I^* and ω^* are the expected amplitude and frequency of the output current of the two-phase orthogonal inverter, respectively.

In order to balance the DC side capacitor voltages, the error of the two capacitor voltages is controlled by a PI controller. The output is Δi . Δi is added to the two-phase inverter output current control. Therefore, the reference two-phase output currents are obtained as:

$$\begin{cases} i_{ref\alpha} = i_\alpha^* + \Delta i \\ i_{ref\beta} = i_\beta^* + \Delta i \\ i_{refw} = -(i_{ref\alpha} + i_{ref\beta}) \end{cases} \tag{20}$$

When one of the power switch devices in the back-stage inverter breaks down, the two-phase 3-brige inverter circuit is reconfigured into a two-phase half bridge inverter circuit. Its corresponding control block diagram is shown in Fig. 11.

The on-off relationship between T_{V12}, T_{V23}, T_{V45}, T_{V56} and the power switch devices is shown in Table II. For example, if the power switch devices V_2 and V_5 are faulty, the back-stage of inverter is reconstructed as a two-phase half bridge inverter circuit according to table I and Fig. 3. It is not necessary to trigger V_2 and V_5. Then T_{V12}, T_{V23}, T_{V45}, T_{V56}, F_{v2} and F_{v5} are off, while F_{v1}, F_{v3}, F_{v4} and F_{v6} are on.

Therefore, when the system operates in the fault condition, it is not necessary to change the control method.

IV. SIMULATION AND EXPERIMENT

A. Simulation Results and Analysis

TABLE III
MAIN PARAMETERS OF THE POWER SUPPLY

Main Parameters	Values
grid voltage/V	380
filter inductor in gird side/mH	1
DC side capacitor /μF	10000
DC side voltage/V	800
switching frequency of IGBT /kHz	10
filter on the output side	L_0=0.5mH
	r_0=0.01Ω
inductor of electromagnetic stirrer/ mH	50
resistor of electromagnetic stirrer /Ω	0.5

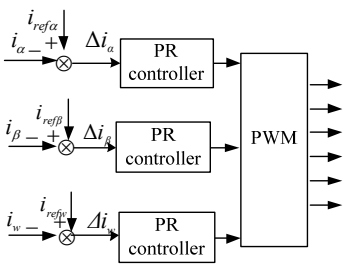

Fig. 12. Control diagram of the back-stage inverter for the traditional structure.

In order to verify the proposed structure and control method, a circuit model of the proposed structure is constructed in PSIM. The main parameters are shown in Table III.

During the operating process, the electromagnetic stirrer operates in the three states of positive rotation, stop and reverse rotation. In order to achieve good electromagnetic stirring performance, the electromagnetic stirrer generates a rotating magnetic field in the clockwise direction by driving the back-stage inverter at 0-0.8s. Then the electromagnetic stirrer stops at 0.8-1.2s. The amplitude of the output current is progressively reduced since the current of the electromagnetic stirring coil cannot be mutated. The electromagnetic stirrer generates a rotating magnetic field in the counter clockwise direction by the inverter at 1.2-2s.

The traditional structure is simulated first with the control method for the back-stage inverter shown in Fig. 12. The control method for the fore-stage rectifier is the same as that of the fault tolerant structure.

Simulation results with the traditional structure and control strategy are shown in Fig. 13-14.

From Fig. 13, it can be seen that when the operating states of the electromagnetic stirrer with the traditional power supply

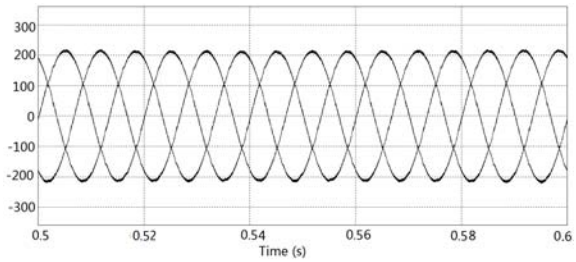

(a) Currents of the PWM rectifier.

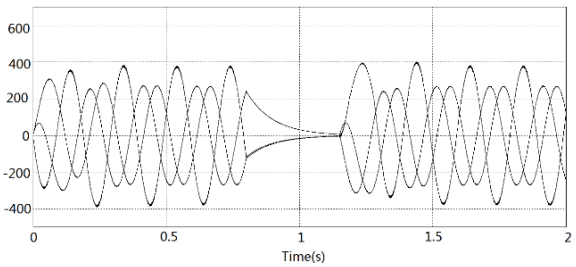

(b) Output currents of the back-stage inverter.

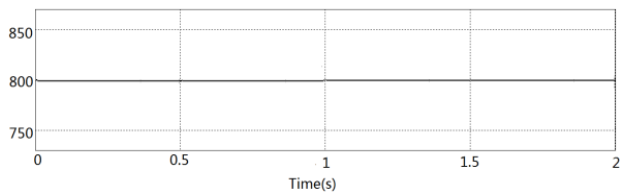

(c) DC side voltage.

Fig. 13. Simulation results under normal operation with the traditional structure and control strategy.

change, the three-phase currents of the fore-stage rectifier are kept sinusoidal. The three-phase output currents of the back-stage inverter are kept in a good shape. The whole DC side voltage is always stable at 800V.

However, if the back-stage inverter with the traditional structure is faulty, the electromagnetic stirrer cannot work normally. The output currents of the back-stage inverter with faulty bridges α, β and w are shown in Fig. 14(b)-(d), respectively. It can be seen in these figures that the two-phase orthogonal currents cannot be obtained. Especially in the stop period, the output currents overflow.

Simulation results with the proposed structure and control strategy are shown in Fig. 15-16.

The simulation results under normal operation with the proposed fault tolerant structure and control strategy are shown in Fig. 15. These figures have the same waves as the traditional structure because of the same structure. The three-phase output currents of the back-stage inverter can track the given currents and keep good shapes. The whole DC side voltage is always stable at 800V.

When one of the power switch devices in the back-stage breaks down, the two-phase 3-bridge inverter circuit is reconfigured into the two-phase half bridge inverter circuit. Fig. 16 shows the simulation results under faulty operation. The results under faulty operation are almost as good as those under normal operation.

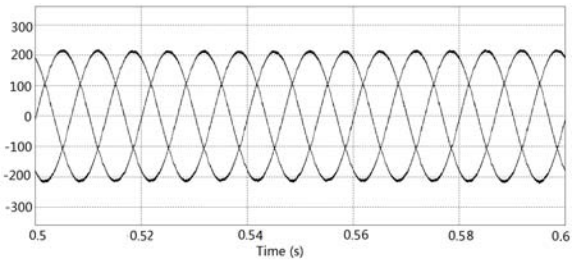

(a) Currents of the fore-stage rectifier.

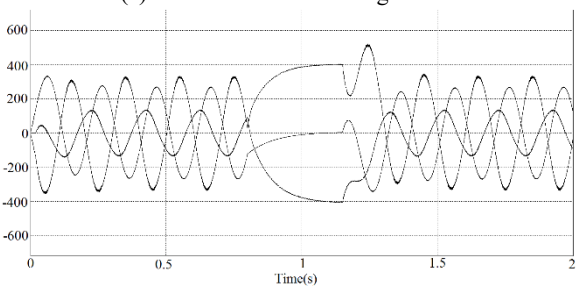

(b) Output currents of the back-stage inverter with a faulty bridge α.

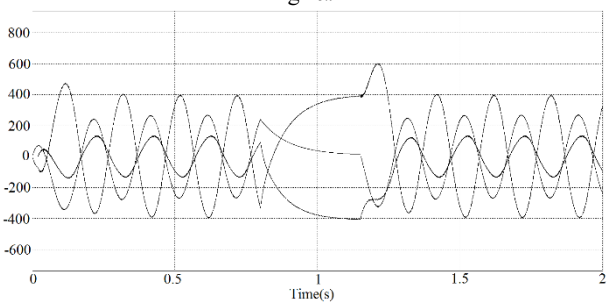

(c) Output currents of the back-stage inverter with a faulty bridge β.

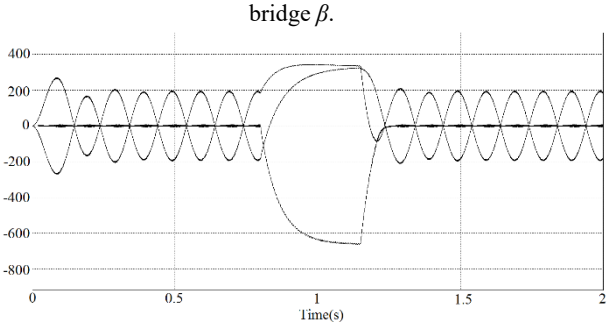

(d) Output currents of the back-stage inverter with a faulty bridge w.

Fig. 14. Simulation results under faulty operation with the traditional structure and control strategy.

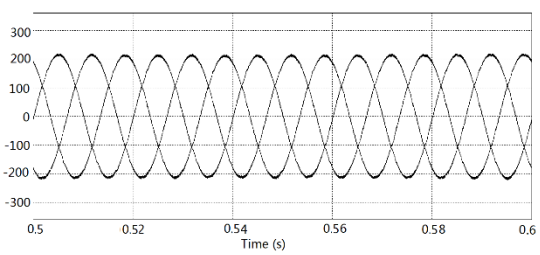

(a) Currents of the fore-stage rectifier.

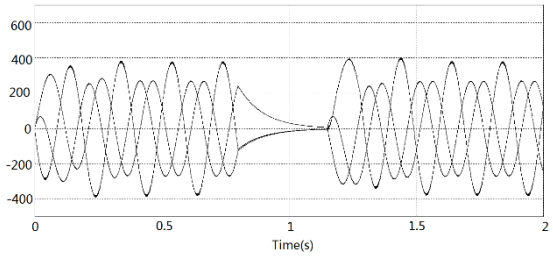

(b) Output currents of the fore-stage rectifier.

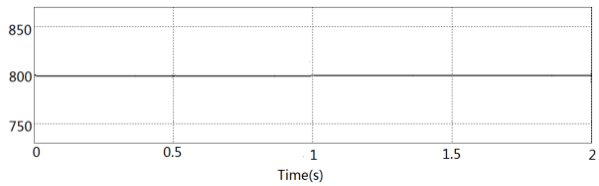

(c) DC side voltage.

Fig. 15. Simulation results under normal operation with the proposed structure and control strategy.

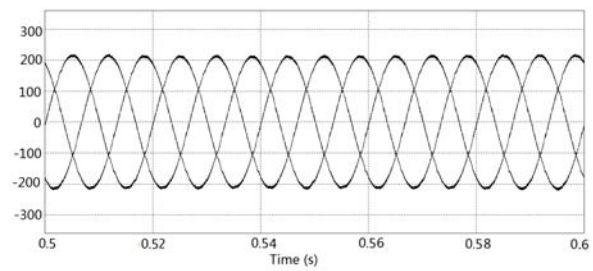

(a) Currents of the fore-stage rectifier.

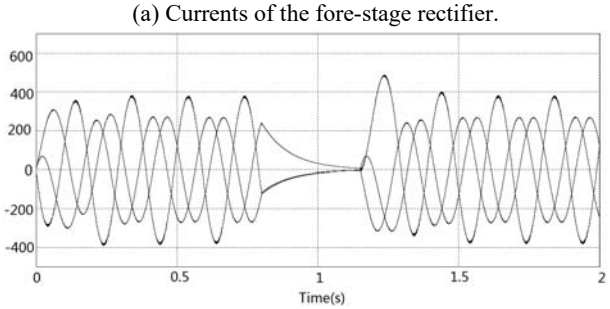

(b) Output currents of the back-stage inverter.

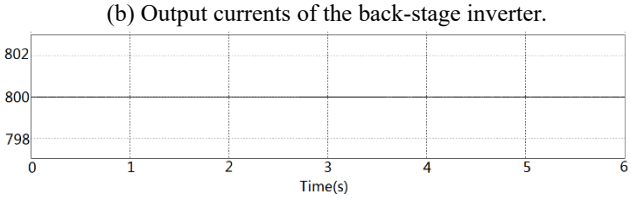

(c) DC side voltage.

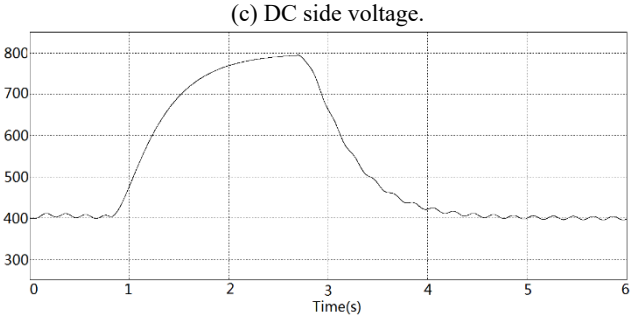

(d) C1 capacitor voltage.

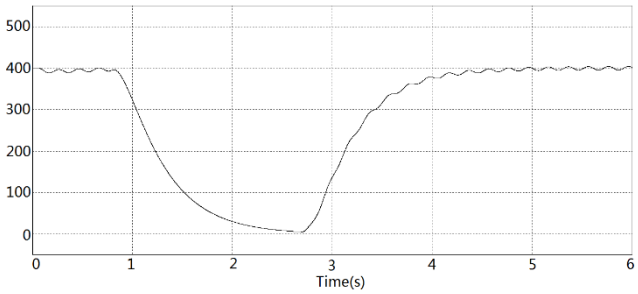

(e) C2 capacitor voltage.

Fig. 16. Simulation results under faulty operation with the proposed structure and control strategy.

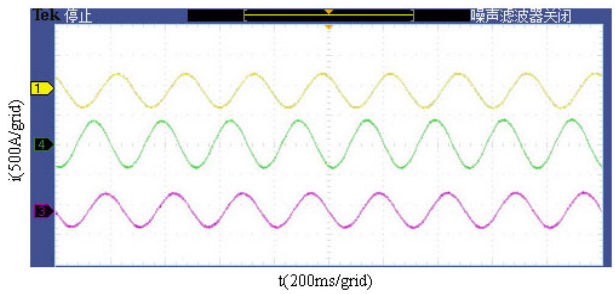

(a) Output currents in positive rotation.

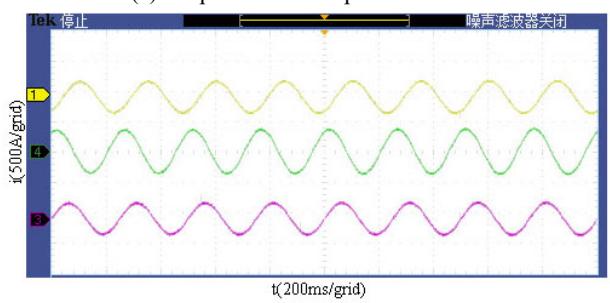

(b) Output currents in reverse rotation.

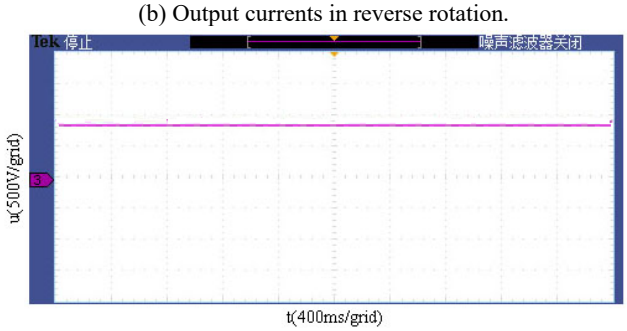

(c) DC-side voltage.

Fig. 17. Experimental results operating in the normal stable condition.

All of the simulation results show that the output currents can quickly track the reference currents and have good shapes. This means that the follow-up trace and precise control by the proposed control strategy are realized under different changing operating conditions. The DC side voltage is kept stable. Therefore, the proposed fault topology and control strategy are feasible according to the simulation results.

B. Experimental Results and Analysis

The proposed fault tolerant topology rated at 300 kVA 380V

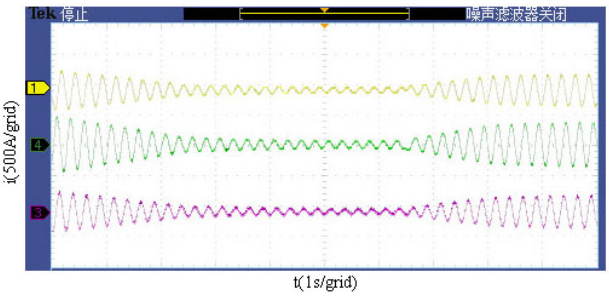

(a) Output currents.

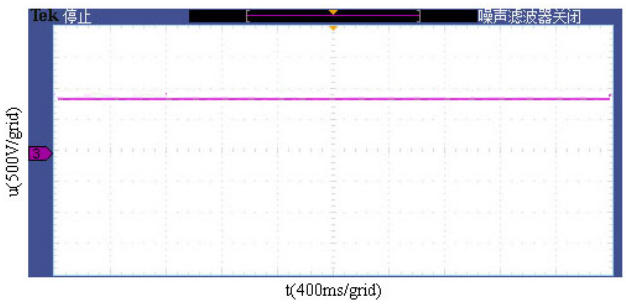

(b) DC-side voltage.

Fig. 18. Experimental results while operating in the normal dynamic condition.

voltage for an electromagnetic stirring power supply and its corresponding control strategy have been implemented. All of the parameters used in the experiments are listed in Table III.

Experimental results while operating in the normal stable condition are shown in Fig. 17. Whether the electromagnetic stirrer is in positive or reverse rotation, the output currents are smooth sinewaves, and track the reference currents correctly. The DC-side voltage wave is stable. The phase difference between the two-phase orthogonal currents is 90°, which are waves 1 and 3 in Fig.17 (a)-(b), corresponding to forward and reverse rotation, respectively.

The experimental results while operating in the normal dynamic condition are presented in Fig. 18. When the electromagnetic stirrer is operated in positive-stop-reverse rotation, the inverter output currents quickly change with the proposed cloud model control method and the current waves are kept good. In addition, the DC side voltage is still stable.

Experimental results obtained while operating under stable and dynamic fault conditions are shown in Fig. 19-20, respectively. From Fig.19-20 it can be seen that the output currents are still sinusoidal in shape when the electromagnetic stirrer is running in the fault condition. The DC side voltage is also stable. These results validate that the proposed topology structure and corresponding control strategy are feasible.

According to the aforementioned results, the proposed topology structure and corresponding control strategy can diminish the DC side ripple voltage caused by the electromagnetic stirrer changing its operating states. The stable control of the power supply is solved. The reliability and performance of the electromagnetic power supply are greatly improved.

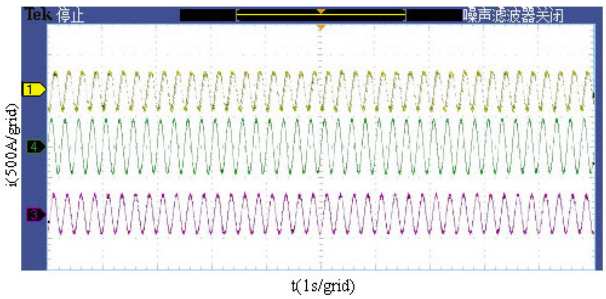

(a) Output currents in forward rotation at 1s/grid.

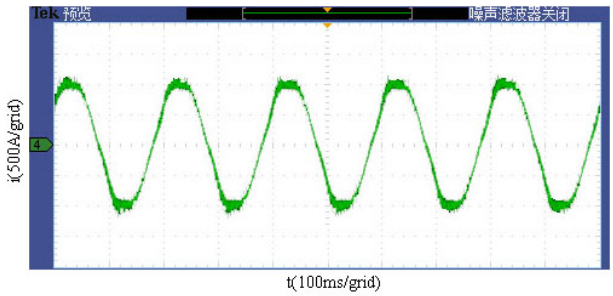

(b) Output currents in forward rotation at 100ms/grid.

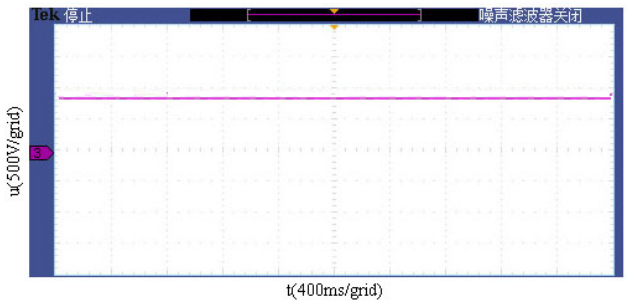

(c) DC-side voltage.

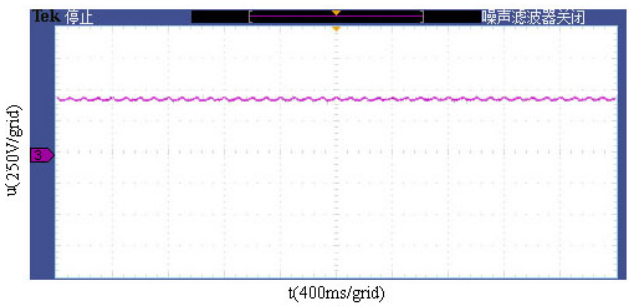

(d) C1 capacitor voltage.

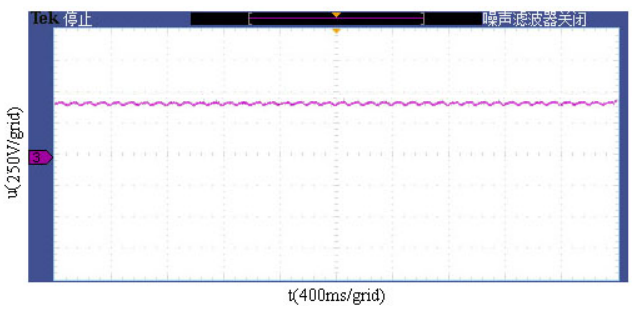

(e) C2 capacitor voltage.

Fig. 19. Experimental results operating in the fault stable condition.

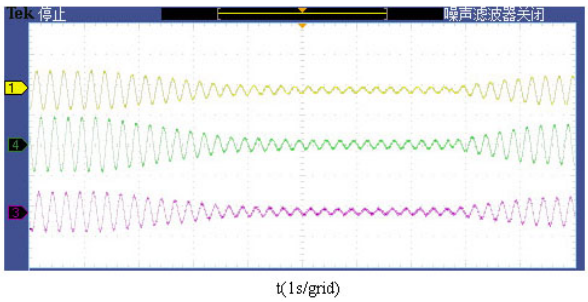

(a) Output currents.

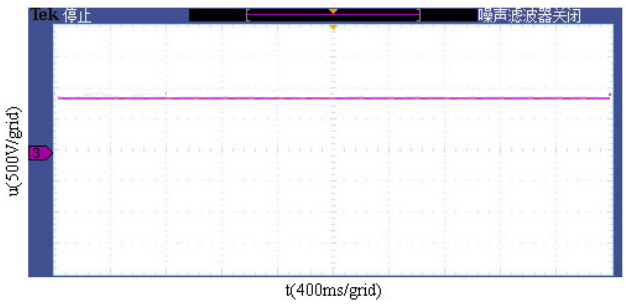

(b) DC-side voltage.

Fig. 20. Experimental results operating in the fault dynamic condition.

V. CONCLUSIONS

A fault tolerant topology structure and its control strategy for electromagnetic stirrer power supplies are proposed in this paper. The back-stage inverter circuit is reconfigured in the faulty condition. After getting rid of the failed power switching devices, the rest of the power switching devices and the DC side capacitor form a two-phase half bridge inverter circuit to keep the system running. There is no coupling between the fore-stage and back-stage of the electromagnetic stirrer power supply. As a result, they can be regarded as two relatively independent control objects. The control strategy is proposed for the electromagnetic stirrer power supplies in this paper. It is not necessary to change control methods in the fault condition. Simulation and experimental results show that the proposed topology and control strategy are correct under normal and faulty conditions.

ACKNOWLEDGMENT

This work was supported by The National Key Research and Development Program of China, project no. 2016YFB0601302, and Science and Technology Major Programs of Hunan Province, China, project no. 2016GK1002.

REFERENCES

[1] C.-T. Liu, “Refined model development and performance assessment of a linear induction-type electromagnetic stirrer,” *IEEE Trans. Magn.,* Vol. 46, No. 10, pp. 3724–3730, Oct. 2010.

[2] C.-T. Liu, S.-Y. Lin, W.-J. Lee, and J.-H. Chen, "Electromagnetic stirring systems," *IEEE Ind. Appl. Mag.*, Vol. 46, No. 2, pp. 38–43, Mar./Apr. 2011.
[3] R. Otake, T. Yamada, and R. Hirayama, "Effects of double-axis electromagnetic stirring in continuous casting," *IEEE Trans. Magn.,* Vol. 44, No. 11, pp. 4517-4520, Nov. 2008.
[4] A. Luo, H. Xiao, H. Ouyang, C. Wu, F. Ma, and Z. Shuai, "Development and application of the two-phase orthogonal power supply for electromagnetic stirring," *IEEE Trans. Power Electron.,* Vol. 28, No. 7, pp. 3438-3446, Jul. 2013.
[5] C. M. Young, C-C. Liu, and C.-H. Liu, "New inverter-driven design and control method for two-phase induction motor drives," *IEEE Proceedings - Electric Power Applications*, Vol. 143, No. 6, pp.458-466, Jun. 1996.
[6] D.-H, Jang, "Investigating carrier-based PWM methods for two-leg, three leg, and four-leg two-phase inverters," *IEEE Ind. Appl. Magn.*, Vol. 13, No. 2, pp. 50–61, Mar./Apr. 2007.
[7] M. A. Chaudhari, H. M. Suryawanshi, and M. M. Renge, "A three-phase unity power factor front-end rectifier for ac motor drive," *IET Power Electronics*, Vol. 5, No. 1, pp. 1–10, Jan. 2012.
[8] D.-H. Jang and D.-Y. Yoon, "Space-vector PWM technique for two-phase inverter-fed two-phase induction motors," *IEEE Trans. Ind. Appl.*, Vol. 39, No. 2, pp. 542-549, Mar./Apr. 2003.
[9] M. A. Jabbar, A. M. Khambadkone, and Z. Yanfeng, "Space vector modulation in a two-phase induction motor drive for constant-power operation," *IEEE Trans. Ind. Electron.,* Vol. 51, No. 5, pp. 1081-1088, Oct. 2004.
[10] D.-H. Jang, "PWM methods for two-phase inverters," *IEEE Ind. Appl. Mag.,* Vol. 13, No. 2, pp. 50-61, Mar./Apr. 2007.
[11] Y. Kumsuwan, S. Premrudeepreechacharm, and V. Kinnares, "A carrier-based unbalanced PWM method for four-leg voltage source inverter fed unsymmetrical two-phase induction motor," *IEEE Trans. Ind. Electron.,* Vol. 60, No. 5, pp. 2031-2041, May 2013.
[12] V. Kinnares and C. Charumit, "Modulating functions of space vector PWM for three-leg vsi-fed unbalanced two-phase induction motors," *IEEE Trans. Power Electron.,* Vol. 24, No. 4, pp. 1135-1139, Apr. 2009.
[13] L. Deyi, M. Haijun, and S. Xuem, "Membership clouds and membership cloud generators," *Journal of Computer Research and Development,* Vol. 32, No. 6, pp. 15-20, Jun.1995.
[14] L. Deyi, "Knowledge representation in KDD based on linguistic atoms," *Journal of Computer Science and Technology*, Vol. 12, No. 6, pp. 481-496, Nov. 1997.
[15] D. Li, "Uncertainty reasoning based on cloud models in controllers," *Computers & Mathematics with Appications*, Vol. 35, No. 3, pp. 99–123, Feb. 1998.
[16] X. Xu, "From cloud computing to cloud manufacturing," *Robotics and Computer-Integrated Manufacturing*, Vol. 28, No. 1, pp. 75–86, Feb. 2012.
[17] X. Wu, R. Zhang, B. Zeng, and S. Zhou, "A trust evaluation model for cloud computing," *Procedia Computer Science,* Vol. 17, pp. 1170–1177, 2013
[18] Y. Li and X. Fan, "Recursive integral proportional–integral control based on membership cloud for active power filter," *IET Power Electronics,* Vol. 7, No. 11, pp. 2870–2876, Nov. 2014.

Yan Li (M'16) was born in Guangxi, China. She received her B.S., M.S. and Ph.D. degrees in Automation, Disaster Prevention and Mitigation Engineering, and Pattern Recognition and Intelligent Systems from Central South University, Changsha, China, in 1999, 2003, and 2007, respectively. She also carried out research in the Electrical Engineering Post-doctoral Research Station of Hunan University, Changsha, China. Her current research interests include microgrids, power quality, power control, and the fault diagnosis of electrical machines.

An Luo (SM'09) was born in Changsha, China, 1957. He received his B.S. and M.S. degrees from Hunan University, Changsha, China, in 1982 and 1986, respectively: and his Ph.D. degree from Zhejiang University, Zhejiang, China, in 1993. In 2003, he became a Professor at Hunan University, where he also serves as the Chief of the National Electric Power Conversion and Control Engineering Technology Research Center. His current research interests include power conversion, harmonics suppression, reactive power compensationn and electric power saving.

Xinxing Xiang was born in Hunan, China, 1983. He received his B.S. degree from the School of Electronic Information, Wuhan University, Wuhan, China, in 2005. He is presently working towards his Ph.D. degree in the College of Electrical and Information Engineering, Hunan University, Changsha, China. His current research interests include model predictive control, static VAR compensators and modular multilevel converters.

Yandong Chen (S'13-M'14) was born in Hunan, China, in 1979. He received his B.S. and M.S. degrees in Instrument Science and Technology, and his Ph.D. degree in Electrical Engineering from Hunan University, Changsha, China, in 2003, 2006 and 2014, respectively. He was an Associate Professor in the College of Electrical and Information Engineering, Hunan University. His current research interests include power electronics for microgrids, distributed generation, power quality, and energy storage. Dr. Chen was a recipient of a 2014 National Technological Invention Awards of China, and a 2014 WIPO-SIPO Award for Chinese Outstanding Patented Invention. He is a Member of the IEEE Power Electronics Society.

Zhixing He (S'15) was born in Hunan, China, in 1989. He received his B.S. degree from the College of Information Science and Engineering, Central South University, Changsha, China, in 2011. He is presently working towards his Ph.D. degree in the College of Electrical and Information Engineering, Hunan University, Changsha, China. His current research interests include model predictive control, static VAR compensators and modular multilevel converters.

Fayun Zhou received his B.S. degree from the Hunan University of Humanities, Science and Technology, Loudi, China, in 2010. He has been working towards his Ph.D. degree at Hunan University, Changsha, China, since 2012. His current research interests include the modulation of multilevel converters and power quality control techniques.

Zhiyong Chen was born in Hunan, China, in 1985. He received his B.S. degree in Automation, and his M.S. degree in Power Electronics and Power Drives from Xiangtan University, Xiangtan, China, in 2007 and 2010, respectively. He received his Ph.D. degree in Electrical Engineering from Hunan University, Changsha, China, where he is presently doing postdoctoral work. His current research interest includes power quality control in distributed generation systems.